J. Fluid Mech. (1998), *vol.* 364, *pp.* 253–272. Printed in the United Kingdom

Driven and freely decaying nonlinear shape oscillations of drops and bubbles immersed in a liquid: experimental results

By E. H. TRINH[1], D. B. THIESSEN[2] AND R. G. HOLT[3]

[1]Jet Propulsion Laboratory, California Institute of Technology, Pasadena, CA 91109, USA
[2]Department of Physics, Washington State University, Pullman, WA 99164, USA
[3]Department of Aerospace and Mechanical Engineering, Boston University, Boston, MA 02215, USA

(Received 10 April 1997 and in revised form 16 January 1998)

Large-amplitude oscillations of drops and bubbles immersed in an immiscible liquid host have been investigated using ultrasonic radiation pressure techniques. Single levitated or trapped drops and bubbles with effective radius between 0.2 and 0.8 cm have been driven into resonant shape oscillations of the first few orders. The direct coupling of driven drop shape oscillations between the axisymmetric $l = 6$ and $l = 3$ modes has been documented as well as the interaction between axisymmetric and non-axisymmetric $l = 3$ and $l = 2$ modes. Effective resonant energy transfer from higher- to lower-order modes has been observed together with a much less efficient energy transfer in the reverse direction. The first three resonant modes for bubbles trapped in water have also been excited, and mode coupling during driven and free-decaying oscillations has been measured. The evidence gathered thus far indicates that efficient drop resonant coupling between a higher- and a lower-order mode occurs when the characteristic frequency of the latter mode roughly coincides with a harmonic resonance.

1. Introduction

Single drop and bubble dynamics are associated with multi-component and multi-phase dispersions occurring in nature and in industrial processes involving liquid–liquid extraction, distillation, or direct contact heat transfer. An improved understanding of the details of the often nonlinear interfacial dynamics should lead to a more accurate modelling of the relevant large-scale processes. In addition, a fundamental understanding of the dynamics will favourably impact the development of methods for the accurate determination of the physico-chemical properties controlling the motion of the drops and bubbles.

The levitation or trapping of single isolated fluid particles allows the control of their position, of their mechanical stimuli, and the accurate measurement of their response. By controlling the time variations of electric or acoustic force fields, contactless static and time-varying shape distortions can be induced and analysed both in the transient as well as steady-state regimes. Practical interest in the deformation and shape oscillations of drops and bubbles immersed in liquid hosts arises because of their impact on particle size distribution in large-scale fluid dispersion systems

through fission and coalescence (Blass 1990; Wright & Ramkrishna 1994). The effects of shape deformation and oscillations on the efficiency of mass and heat transport have also been investigated in the past using translating fluid particles in a liquid or gaseous host (Kawalski & Ziolkowski 1981; Kaji *et al.* 1985; Scott, Basaran & Byers 1990). The observed increase in the transport rates of oscillating drops cannot be attributed to the increase in surface area alone. Rather, the details of the dynamics of the shape oscillations and their impact on the fluid circulation around and inside the drops or bubbles are believed to play the primary role in this enhancement.

Because of inter-particle collision and flow perturbations, the shape deformations of individual droplets and bubbles in dispersions are often large, and the resulting shape oscillations are consequently nonlinear. Theories based on small-amplitude approximations (Rayleigh 1879; Lamb 1881; Miller & Scriven 1968; Prosperetti 1980; Marston 1980) cannot accurately describe the details of the dynamics in this amplitude range. The fundamental characteristics of nonlinear inviscid drop shape oscillations have been addressed by Tsamopoulos & Brown (1984) through multiple-time-scale expansion and by Natarajan & Brown (1986) who derived the equations describing the nonlinear interaction of resonant modes by using the variational principle for the Lagrangian of the oscillatory motion. The quadratic and third-order couplings of axisymmetric resonant modes of charged drops freely suspended in a tenuous medium (vacuum or gas) were considered in the former study, and uncharged drops were treated by the latter authors. The principal predictions obtained were the quadratic decrease of the drop and bubble resonant mode frequencies as a function of the oscillation amplitude, and the resonant coupling of modes whose frequencies are integer multiples. Such modal interactions have been characterized by either aperiodic or periodic modulations of the amplitude and phase of the interacting modes. Experimental corroboration has been obtained for the amplitude dependence of the fundamental mode resonance frequency for drops suspended in liquid and in air, but no evidence for soft nonlinearity in the resonance frequency has yet been provided for the case of bubbles in liquids. Similarly, no experimental evidence for nonlinear modal coupling has yet been presented for drops and bubbles immersed in a liquid. In this paper, we will address some of these particular issues by presenting experimental observations of modal coupling of the resonant modes of both drops and bubbles immersed in a liquid host and driven into shape oscillation by the modulation of the ultrasonic radiation pressure.

2. Experimental approach

In this work, we use a primary ultrasonic standing wave to support a drop or trap a bubble against gravity, and we modulate this wave at a vastly lower frequency to drive the drop into shape oscillations. A technique developed for previous experimental studies of linear and nonlinear drop (Marston & Apfel 1979; Trinh, Zwern & Wang 1982; Trinh & Wang 1982) and bubble shape oscillations (Asaki, Marston & Trinh 1993) has thus been used to gather the data reported in this paper. This particular implementation of the acoustic levitation method has thus been previously described in detail, and only a cursory discussion will be presented here. As shown in figure 1 a liquid-filled cell with square cross-section is excited into resonance through direct coupling to the piezo-electric transducer attached at its bottom. A specific three-dimensional ultrasonic standing wave in the liquid column is excited near the fundamental longitudinal (length) mode of the transducer (around 22.5 kHz) or at one of its odd harmonics (around 66 kHz). The empirical frequency matching

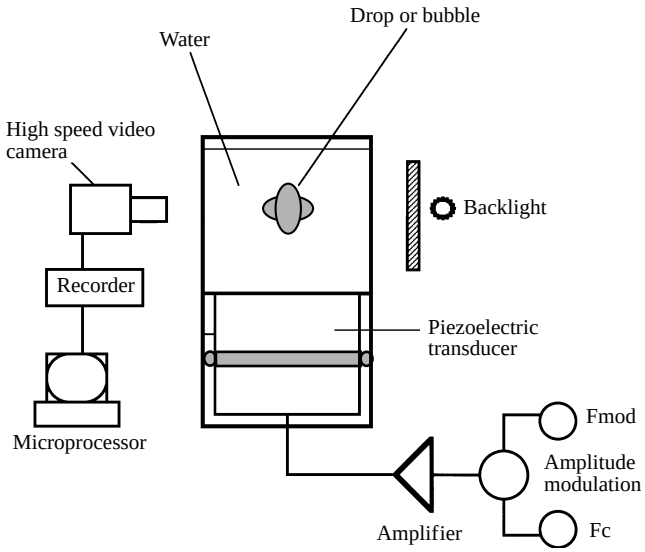

FIGURE 1. Schematic description of the experimental apparatus. A Lucite square-cross-section cavity has been machined to allow the mounting of a resonant piezoelectric transducer at the bottom of the chamber. This transducer is driven by a function generator and amplifier in order to establish a three-dimensional standing wave in the water-filled chamber. This standing wave is amplitude modulated in order to modulate the acoustic radiation pressure to drive the levitated drops and trapped bubbles into shape oscillations. The data described in this paper have been acquired through the analysis of digitized frames from a high-speed video camera recording the dynamics of the backlighted fluid particles.

of these two resonances is carried out by varying the height of the liquid column, and a typical desirable resonant mode provides isolated three-dimensional acoustic pressure nodes and antinodes near the cell axis of symmetry. Liquid drops which are more compressible than the host liquid are driven toward and levitated near pressure antinodes (Apfel 1976), and gas bubbles which are smaller (larger) than resonant size are driven toward and trapped near pressure antinodes (nodes) (Eller 1968). The bubble resonant size is that at which the volumetric bubble resonance frequency is equal to that of the standing wave. This volumetric mode frequency ω_R (the Minnaert frequency) is approximately given by

$$\omega_R^2 = \frac{3\gamma P_0}{\rho R^2} - \frac{2\sigma}{\rho R^3}, \tag{2.1}$$

where γ is the ratio of the specific heats of the gas, P_0 is the ambient hydrostatic pressure, σ the surface tension, ρ is the liquid density and R the equilibrium bubble radius. For the bubble sizes of interest in this study, the second term on the right-hand side is small compared to the first term.

In this paper we report results obtained with both drops and bubbles, the latter always larger than resonant size, and trapped slightly above a local pressure node. An experimental study of the large-amplitude oscillations of drops levitated in air and under the combined action of electric and ultrasonic fields has been reported elsewhere (Trinh, Holt & Thiessen 1996).

Modulation of the acoustic radiation stresses acting on the interface has provided the drive for the shape oscillations. This was primarily carried out through direct modulation of the fundamental levitation standing wave, but the amplitude modula-

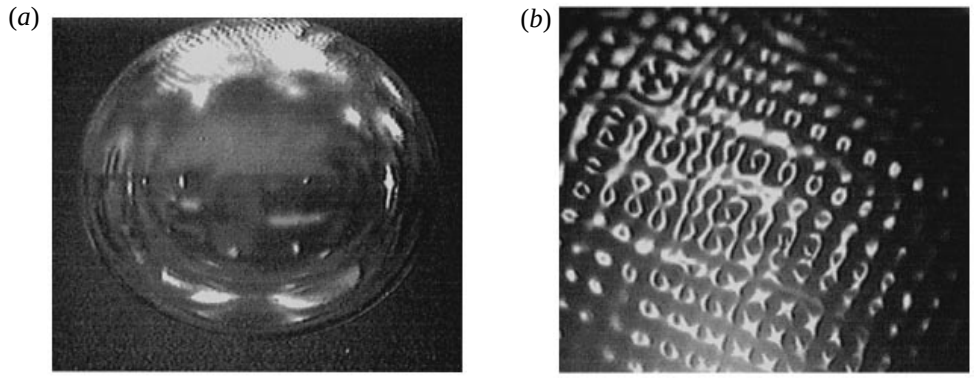

FIGURE 2. (*a*) Backlit image of a trapped 4.5 mm diameter air bubble in water. The structure faintly seen at the north pole is high-frequency capillary waves excited through the Faraday instability on the air–water interface. (*b*) Higher-resolution video frame of the capillary waves at the bubble north pole. The waves have been recorded with a video camera with high-intensity short-duration pulsed lighting.

tion of the third harmonic has also been implemented in order to provide a greater stress on the individual fluid particles. For the amplitude modulation of the radiation pressure, the voltage across the ultrasonic transducer, V_{ac}, is given by

$$V_{ac} = V_{ac0}\,[1 + M\cos(\omega_m t)]\cos(\omega_{ac} t)\,, \tag{2.2}$$

where V_{ac0} is the amplitude of the carrier voltage at the frequency $\omega_{ac} = 2\pi f_{ac}$ for the acoustic standing wave ($f_{ac} = 22.5$ kHz), M is the modulation index for the amplitude modulation of the acoustic force at the frequency ω_m. Because the acoustic radiation force is proportional to the square of the acoustic pressure, this force is therefore proportional to V_{ac}^2, and this amplitude modulation results in a time-varying acoustic force at both the frequencies ω_m and $2\omega_m$. This results in a *periodic flattening of the drop or bubble by the acoustic force* when the fluid particle diameter is small compared with the ultrasonic wavelength. When the particle diameter is a significant fraction of the ultrasonic wavelength, however, the periodic elongation of the drop or bubble along the vertical axis can also be obtained through amplitude modulation of the acoustic pressure. A static distortion of the drop or bubble can also be induced by the ultrasonic levitation or trapping field as the size of the fluid particle becomes a non-negligible fraction of the wavelength. Figure 2(*a*) shows the unmodulated shape of a large air bubble of approximately 0.8 cm in diameter trapped in a 22.9 kHz sound field. In addition to the shape asymmetry with respect to the equator, one can also notice the presence of short-wavelength capillary waves on the upper hemisphere of the trapped bubble. Figure 2(*b*) is a magnified image obtained under short duration stroboscopic illumination and shows the capillary waves in greater detail. The frequency of these waves has been determined to be around 11 kHz, indicating that the generating mechanism is probably through the Faraday instability (Holt & Trinh 1994). This has also been shown to induce resonant shape oscillations for smaller bubbles (10–30 μm in diameter) which are initially acoustically driven in the radial mode (Holt & Gaitan 1996). The presence of these capillary waves and the fact that the equilibrium shape of the trapped bubbles is not spherical both influence the characteristics of the shape oscillations. The details of such effects are beyond the scope of this paper, however, but they will be addressed in

FIGURE 3. Single video frames displaying the light scattered from a trapped air bubble containing suspended tracer particles. A steady-state streaming flow can be observed within the air bubble. The velocity distribution is highly non-uniform because the principal driving mechanism for streaming appears to be the capillary waves at the bubble top surface.

a forthcoming low-gravity investigation to be carried out using a similar experimental apparatus.

An acoustically induced steady-state convective flow field is also present in the gas inside the trapped bubble as shown in figure 3. This time-exposure photograph of both a trapped bubble and its immediate surrounding shows steady and oscillatory circulation both inside and outside the bubble (in the air and in the liquid). The flows have been visualized using incense smoke particles inside the bubble and polymer particles suspended in the surrounding liquid. They are illuminated by a laser sheet, and the scattered light is recorded by a video camera. The outer streaming in the liquid has been documented previously and is expected, but the inner flow has not been seen before and is under more detailed scrutiny. The results will be reported in a later publication.

The driven and freely decaying shape oscillations of both drops and bubbles were monitored by standard (30 frames/second) and high-speed (2000 frames/second) video cameras. To facilitate the automated analysis of the drop or bubble shapes from the digitized individual video frames, backlighting was selected as the primary illumination technique. The high-contrast, dark contours in a bright background were analysed with an edge-finding routine, and the experimental data were fitted into axisymmetric shapes with the usual expansion in terms of the time-dependent surface spherical harmonics.

The shape of the drop or bubble, described by $R(\theta, t)$ is expanded as

$$R(\theta, t) = R_0 \left[1 + \sum_{l=2}^{l^*} c_l(t) P_l(\cos\theta \right], \tag{2.3}$$

where R_0 is the radius of the sphere of the same volume, $P_l(\cos\theta)$ is the Legendre polynomial of degree l, and $c_l(t)$'s are the corresponding coefficients. Using this method we can obtain the time series for each $c_l(t)$ for driven and freely decaying shape oscillations. For the data described in this paper, we have limited ourselves to $l^* = 6$. A digitally analysed video frame contains up to a maximum of 320×240 pixels and in 256 levels of grey. Figure 4 shows a series of shapes recorded on still video for a drop initially driven into the axisymmetric $l = 3$ mode and subsequently exciting the non-axisymmetric $l = 2$ mode. This case is discussed in a later section of this paper. Figure 5 shows the photographs of the extremum shapes of a drop initially driven into the $l = 6$ mode and subsequently exciting the $l = 3$ mode. This

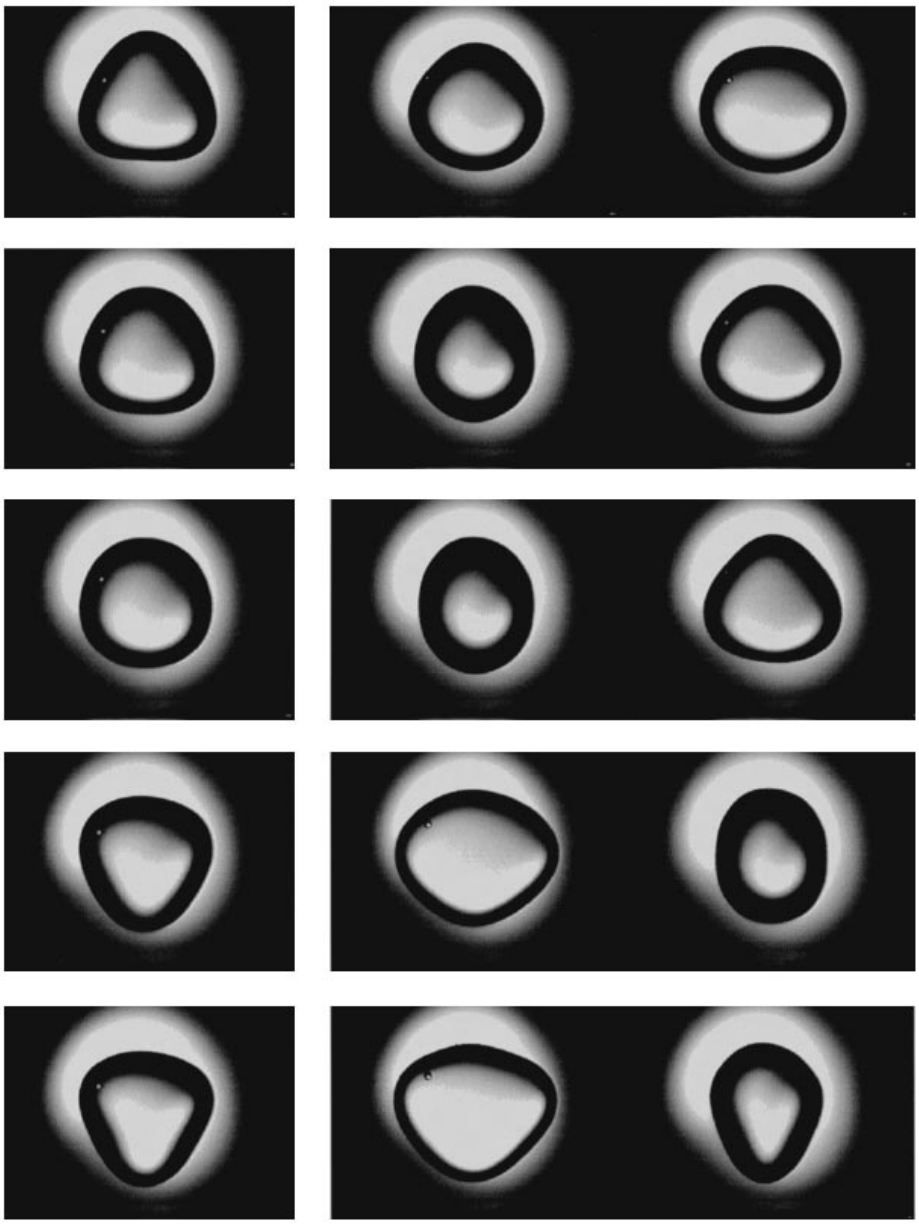

FIGURE 4. Series of video single frames of a silicone oil drop in water initially driven into the axisymmetric $l = 3$ mode. Non-axisymmetric $l = 2$ oscillations are gradually excited through harmonic resonance. The initial axisymmetric three-lobed oscillations are coupled with oblate-prolate shapes as shown on this view perpendicular to the original axis of symmetry. The series of five pictures on the left depicts axisymmetric $l = 3$ mode shapes. The series of ten pictures on the right shows shapes of superposed $l = 3$ and $l = 2$ oscillations.

case is also discussed in the following section. The illumination used for the drop photographs is a combination of back and side lighting.

The materials used for these studies are silicone oil (Polydimethylsiloxanes) with a kinematic viscosity of 2 cSt for the drops and distilled outgassed water for the host

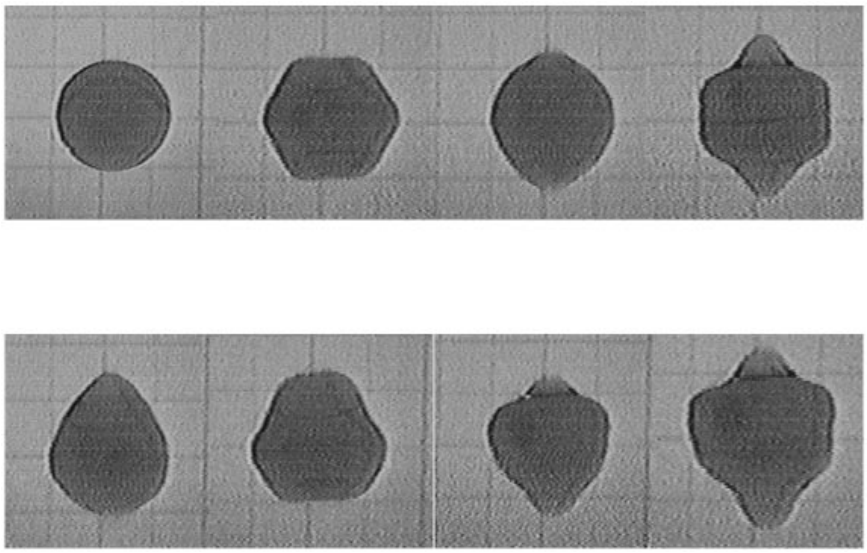

FIGURE 5. Series of video single frames showing the shapes of an initially axisymmetric $l = 6$ (top row) and the shapes of the superposed $l = 6$ and $l = 3$ shape modes (bottom row). The $l = 3$ secondary oscillations are excited by the large-amplitude acoustically driven $l = 6$ mode. Characteristic three-lobed configurations are seen superposed on the original six-lobed geometry.

liquid. The drop diameter ranged from 1.0 to 1.5 cm, and the ultrasonic frequencies of the standing waves used to excite the shape oscillations were 22.5 and 66 kHz.

3. Experimental results

3.1. *Drop shape oscillations*

The first few driven resonant shape oscillations of drops immersed in a liquid host have been previously observed by using ultrasonic radiation pressure (Marston & Apfel 1979; Trinh *et al.* 1982; Annamalai, Trinh & Wang 1985) and electric field drive (Rhim, Elleman & Saffren 1982; Scott *et al.* 1990; Azuma, Yoshihara & Ohnishi 1989). Although the controlled excitation and measurement of the well-resolved and independent resonant modes and the experimental evaluation of the weak nonlinear characteristics of the fundamental quadrupole (oblate-prolate) mode has allowed the validation of both the linear theory and predictions from nonlinear numerical calculations (Tsamopoulos & Brown 1984), no data on resonant mode coupling have yet been published. In this paper we report observations of the interaction between resonant modes when their nominal resonant frequencies satisfy an approximate integer multiple relationship. The strongest coupling has been found for a 2:1 ratio where a mode is initially acoustically driven at high amplitude, and a lower-order mode is subsequently excited at a sub-harmonic frequency due to nonlinear interaction.

3.1.1. *Coupling between $l = 3$ and $l = 2$ modes*

Figure 6 summarizes the experimental results for a 1.1 cm diameter silicone oil drop in water. The videotape frames capturing the drop motion were digitized and the drop contour on each frame was continuously fitted with 100 points. Assuming axial symmetry, this drop boundary was decomposed into shapes associated with Legendre polynomials. These coefficients (between $c2$ and $c6$) are plotted in figure 6.

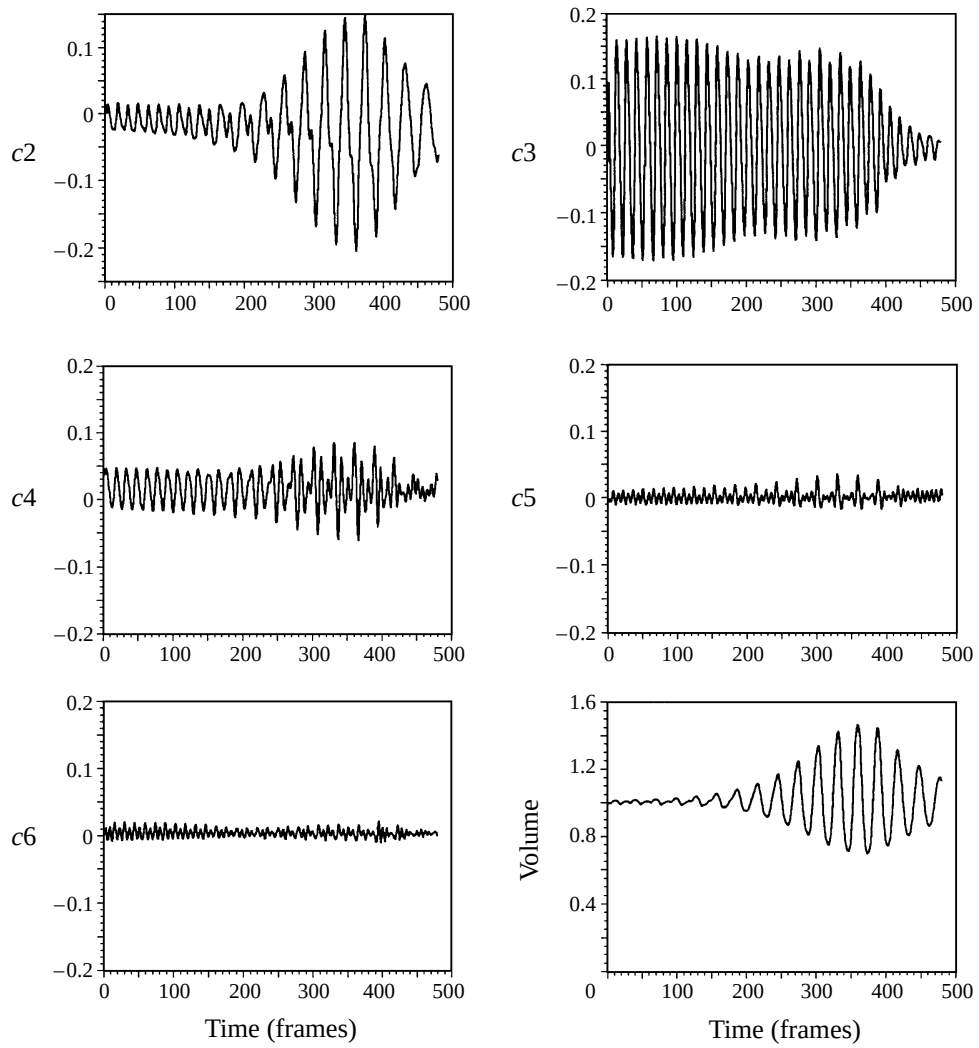

FIGURE 6. Time-dependence of the first five Legendre coefficients of a 1.1 cm diameter silicone oil drop levitated in water and initially driven into the axisymmetric $l = 3$ resonant mode of shape oscillations. The sub-harmonic excitation of a non-axisymmetric $l = 2$ resonant mode is the salient characteristic. A strong harmonic component can also be detected in the $c4$, $c5$, and $c6$ Legendre coefficients.

The volume is calculated assuming axial symmetry, and is also plotted in order to check the constant-volume restriction.

In this particular measurement, the drop was initially driven in the $l = 3$ axisymmetric mode resonance (at 2.15 Hz) at large amplitude (20% of the drop diameter). The steady-state oscillations are characteristically three-lobed and they can be viewed along a horizontal view axis (see figure 4), while an oscillating circular cross-section can be seen along the orthogonal vertical axis (symmetry axis). This is confirmed by the plot of the volume which shows a constant value centred at 1.0. At about 150 frames, the amplitude of the $l = 2$ mode Legendre coefficient ($c2$) begins to increase, and displays a sub-harmonic time-dependence at 1.07 Hz. These $l = 2$ mode oscillations grow in amplitude at the expense of the $l = 3$ oscillations, but they are

not axisymmetric along the vertical axis. Rather, they are aligned along a horizontal direction normal to the symmetry axis. This is reflected by the deviation of the calculated volume from unity. The acoustic shape oscillation drive is removed after 360 frames, and the decay of all the shape oscillation modes can be observed.

Although the assumption of axial symmetry is obviously violated as shown by the apparent volume variations, we can nevertheless accurately identify the specific coupled resonant modes through visual observations. The axisymmetric $l = 3$ three-lobed oscillations (at 2.15 Hz) can be viewed along one axis while the drop cross-section remains circular along the orthogonal view (along the symmetry axis). As the $l = 2$ mode becomes excited, oblate-prolate oscillations (at 1.07 Hz) can be seen along the orthogonal axis, and the previously three-lobed oscillations are modulated by these oblate-prolate oscillations. Although the superposed oscillations are no longer axisymmetric, the composite motion can still be visually decomposed into two separate components with separate symmetry axes and different, but harmonically related frequencies.

This combination of visual analysis of the video data with the quantitative analysis of the digitized images is very effective at the low oscillation frequencies (1–5 Hz) characteristic of the relatively large drops used in this study.

One might note that according to linear theory results (Marston 1980), the ratio of the small-amplitude resonance frequencies $\omega 3/\omega 2$ is near 1.82 for the current conditions and for axisymmetric modes (the theoretical value for the $l = 2$ mode is 1.18 Hz). This was found to be in closer agreement with experimental results than the corresponding theoretical value of 2 for the inviscid case (Trinh *et al.* 1982). We, therefore, use Marston's theoretical values for the resonant mode frequencies throughout this paper, keeping in mind that they strictly only apply to axisymmetric small-amplitude oscillations.

The lower frequency value corresponding to the sub-harmonic coupling observed here (1.07 Hz), could be explained by the detuning due to viscous effects, or it might correspond to a lower resonance frequency for the non-axisymmetric mode which has been excited in this particular case. Viscous dissipation decreases the quality factor (or Q) of resonant systems and resonant oscillations can be driven with a significant amount of detuning. In the present case, the typical Q of a drop in water is on the order of 10 for the fundamental ($l = 2$) and least-damped mode, and the observed detuning of 10% would not exclude a coupling mechanism based on harmonic resonance.

The removal of the degeneracy for resonant drop shape oscillations has been observed experimentally: three different $l = 2$ modes can be driven at slightly different frequencies grouped around the theoretically predicted resonance. An analysis of the removal of the degeneracy by a static shape deformation is also available in the literature (Suryanarayana & Bayazitoglu 1991). In previously reported experimental results on drops levitated in air (Trinh *et al.* 1996), three separate $l = 2$ modes were also observed, and a non-axisymmetric mode was found to have the lowest frequency. If the same is true for this case, the frequency ratio of the axisymmetric $l = 3$ mode to the non-axisymmetric $l = 2$ mode would be closer to 2.

In figure 7 are plots of Fourier transforms of the time-dependent Legendre coefficients, which show the frequency spectrum for each Legendre shape. The Fourier transforms were calculated using all the data shown in the time-dependence plots. The first obvious characteristic is the presence of the initial driven frequency 2.15 Hz of the $l = 3$ mode on all of the spectra for the corresponding Legendre coefficients. This indicates that large-amplitude oscillations in an initially pure mode will drive

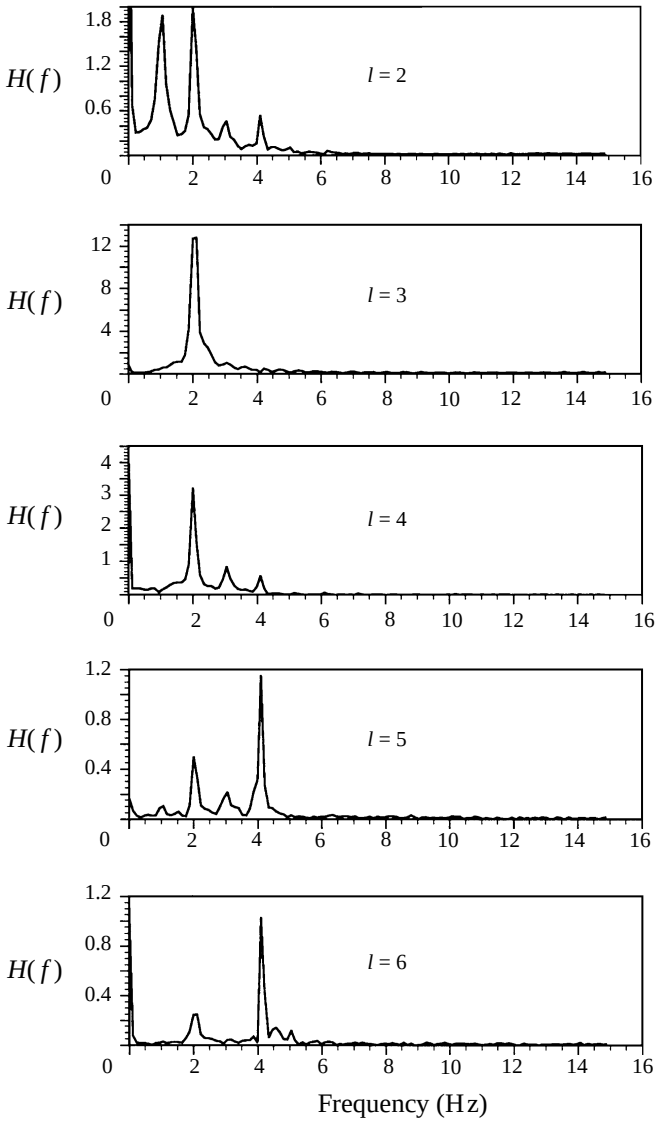

FIGURE 7. Fourier spectra of the times series shown in figure 6. Both sub-harmonic and harmonic components are prominently displayed. All the data points shown in the time series have been used in the Fourier transform operation.

motion which has other characteristic higher-order mode shapes all having the same initial driven frequency. This was predicted by Feng & Beard (1990, 1991) when they considered the case of electrically driven oscillations of charged drops in a gas. Interestingly, the sub-harmonic frequency strongly appears only in the $l = 2$ and somewhat weakly in the $l = 5$ mode spectra. Another salient characteristic is the excitation of a near second-harmonic component at 4.2 Hz corresponding to the $l = 5$ mode oscillations. The theoretical $l = 5$ mode linear resonance frequency is roughly twice that of the $l = 3$ mode (4.3 Hz).

Also significant is the fact that we have not been able to get a strong coupling in the reverse direction, i.e. it has not been possible to drive the $l = 3$ mode at

its characteristic resonance frequency by acoustically exciting the axisymmetric or non-axisymmetric $l = 2$ oscillations. Large-amplitude driven $l = 2$ motion generates $l = 3,4,5,6$ shapes at its driven frequency as well as its harmonics. For example, the $l = 3$ oscillatory shapes have the frequency of the driven $l = 2$ mode, and $l = 4$ oscillations are found to have frequency components at $f(l = 2)$ and at $2f(l = 2)$ instead of $3f(l = 2)$ as prescribed by linear theory. This appears to agree with previously published results based on a nonlinear analysis of the decay of drops released from a nozzle (Becker, Hiller & Kowalewski 1994).

These results can be summarized as follows: (i) large-amplitude acoustically driven resonant oscillations in a pure mode can sub-harmonically excite a corresponding resonant mode having different symmetry characteristics; (ii) they generate the first few of the Legendre axisymmetric shapes at the same driving frequency; and (iii) they can also drive higher-harmonic resonant mode oscillations (second harmonic in this case) as predicted by Tsamopoulos & Brown (1984).

3.1.2. *Coupling between the $l = 6$ and $l = 3$ modes*

In this second case, a 1.5 cm diameter silicone oil drop was levitated in distilled water and driven into resonant $l = 6$ mode oscillations (see figure 5). Figure 8 shows the initial driven motion of the $c6$ Legendre coefficient at 6.7 Hz, the rising amplitude of the $c3$ coefficient, and the steady driven $l = 3$ oscillations at the sub-harmonic frequency of 3.4 Hz. A slight non-axisymmetric component at the same sub-harmonic frequency is detected in the plot of the calculated volume as a function of time. Also observable is the rising prominence of the sub-harmonic frequency (3.4 Hz) in the time-dependence of both the $c2$ and $c4$ coefficients. Figure 9, showing the plots of the Fourier transform of the Legendre coefficients, confirms the presence of the driving and sub-harmonic frequencies. The second-harmonic frequency component is not apparent in this case because the resonant mode response at such a high frequency (13.4 Hz) is highly damped by viscosity.

One must note, however, that the calculated small-amplitude normal mode frequency ratio $\omega 6/\omega 3$ is approximately equal to 2.5, not 2.0, i.e the theoretical resonance frequency for the $l = 3$ mode is only 2.7 Hz. In this case, the observed sub-harmonic frequency of the secondary (nonlinearly driven) mode is higher than the theoretical small-amplitude resonant $l = 3$ mode frequency. Thus, there appears to be a significant degree of detuning in the sub-harmonic drive of the $l = 3$ characteristic mode. This is not surprising owing to the increased viscous damping associated with the higher-order modes. In addition, because of the soft nonlinearity of large-amplitude shape oscillations, the actual frequency of maximum response for the $l = 6$ mode is shifted to a value lower than the resonance frequency predicted by the linear theory. The experimental frequency ratio would also be smaller than 2.5 when previous experimental results and theoretical predictions are taken into account (Tsamopoulos & Brown 1983; Trinh & Wang 1982).

Here again, harmonic resonance appears to be the logical explanation for the observed drop behaviour, and sub-harmonic coupling is the dominant mechanism which can also be logically explained by the influence of viscous dissipation. In this case, the $l = 3$ mode did not transfer energy to the non-axisymmetric $l = 2$ mode as observed in the previously described data. Instead, the axisymmetric $l = 2$ mode is initially excited very weakly by the acoustically driven $l = 6$ oscillations, and more significantly by the nonlinearly driven $l = 3$ mode. The influence of a driven mode appears clearly to be substantial for neighbouring ones, but is less apparent for more distant modes. The $l = 2$, 4, and 5 modes all display an initial time dependence at

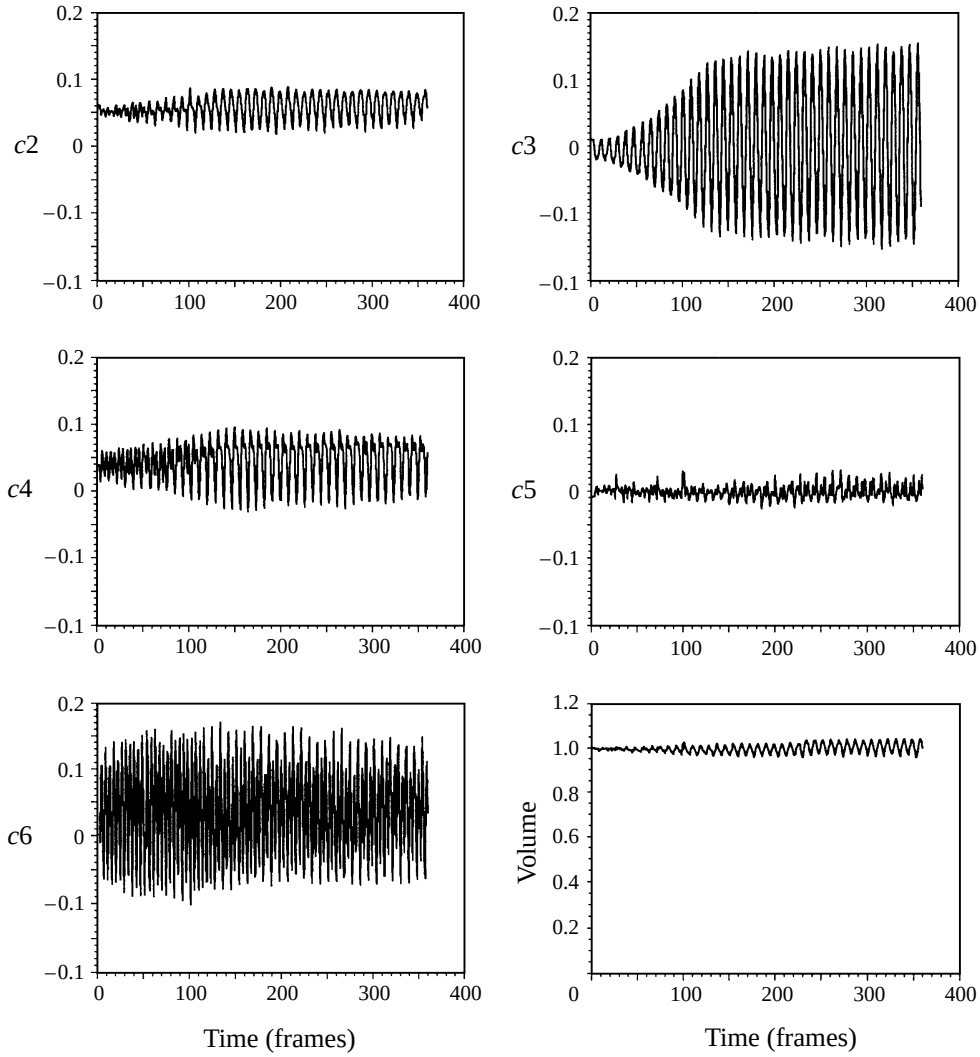

FIGURE 8. Time-dependence of the first five Legendre coefficients for a 1.5 cm diameter silicone oil drop levitated in water and initially driven into the $l = 6$ resonant mode of shape oscillations.The sub-harmonic coupling leads to the excitation of the resonant $l = 3$ mode accompanied by a very slight decrease in the amplitude of the response in the $l = 6$ mode.

the driven $l = 6$ mode frequency, but the $l = 2$ and 4 modes time response becomes dominated by the $l = 3$ mode as the latter rises to larger amplitude. Meanwhile, its effect on $l = 5$ and $l = 6$ modes is relatively minor.

3.1.3. *Coupling between the $l = 4$ and $l = 2$ modes*

In this third case, a 1.2 cm diameter silicone oil drop in distilled water was initially driven into resonant $l = 4$ axisymmetric oscillations at 4.6 Hz (see the $c4$ coefficient plotted as a function of time in figure 10). The fairly large amplitude driven oscillations in the $l = 4$ mode appear to excite even numbered oscillations ($l = 2$ and $l = 6$) at the same frequency, but they do not appreciably induce odd-numbered mode motion ($l = 3$ and $l = 5$). This is in agreement with predicted behaviour (Feng & Beard 1990).

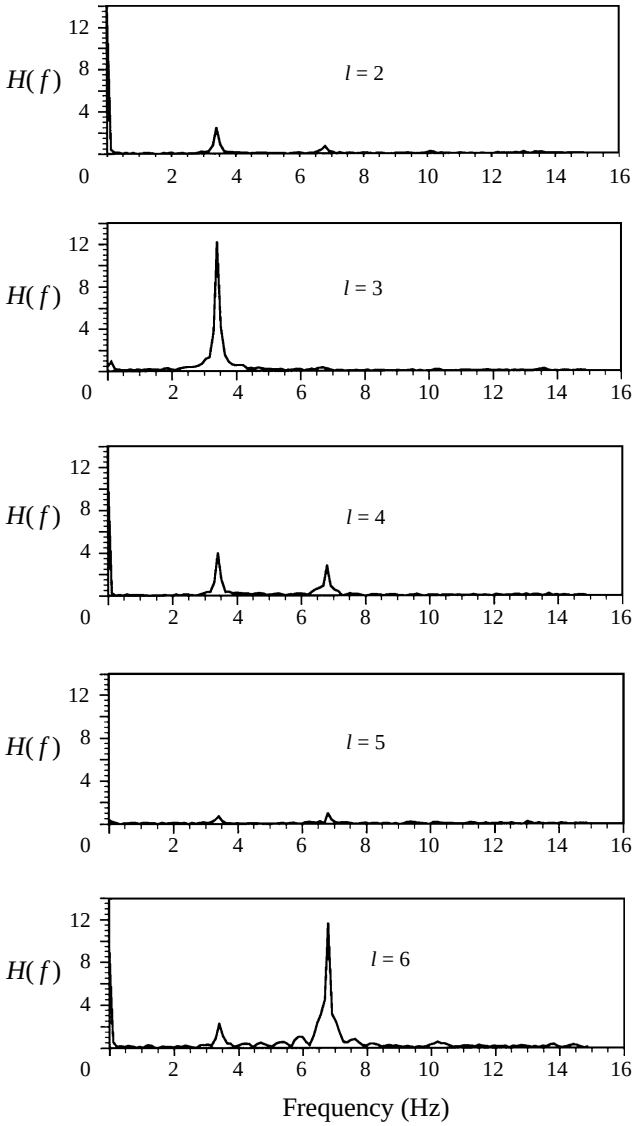

FIGURE 9. Fourier transforms of the data in figure 8 prominently display that sub-resonant coupling. All the data points shown in the time series have been used in the Fourier transform operation.

The apparent contradiction raised by the cases discussed in the preceding sections could be rationalized by invoking harmonic resonance. The time-dependence of the $l = 2$ mode motion is a superposition of two frequencies: the quadrupole oscillations at 2.3 Hz and the driving frequency of the $l = 4$ mode at 4.6 Hz. Also note that the $l = 2$ mode oscillations are about a substantially oblate equilibrium configuration (the value of the $c2$ coefficient is negative throughout the shape oscillations).

According to linear theory for spherical drops, the ratio of the $l = 4$ to $l = 2$ mode frequencies is about 2.6, although the actual frequency ratio for large-amplitude oscillations will be lower for the same reasons mentioned in the preceding case. The theoretical resonance frequency for the $l = 2$ mode is 1.77 Hz. The amount of detuning is thus even larger than in the preceding case, and it could explain

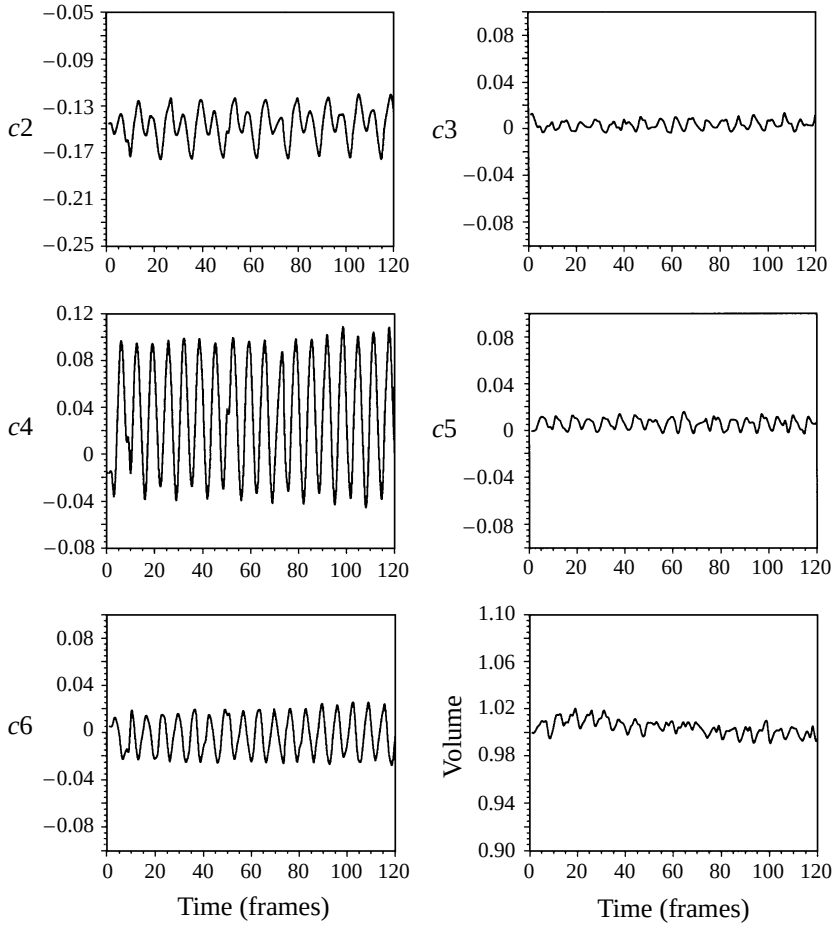

FIGURE 10. Time-dependence of the Legendre coefficients for a 1.2 cm diameter silicone oil drop levitated in water and initially driven into the $l = 4$ resonant mode of shape oscillations. Sub-resonant excitation drives the $l = 2$ mode which responds at a combination of the driving and sub-harmonic frequencies.

the relatively weaker observed coupling. Although sub-harmonic resonance is still observed, the harmonic coupling between these two particular modes is weaker than in the preceding two cases.

3.2. *Bubble shape oscillations*

Shape oscillations have been experimentally studied in the past in the context of the shape stability of radially oscillating small bubbles: as the amplitude of the volume oscillations of bubbles trapped in an ultrasonic standing wave increases, resonant surface standing waves (shape oscillations) are parametrically excited through the Faraday instability mechanism (Strasberg & Benjamin 1958; Eller & Crum 1970; Benjamin & Ellis 1990; Feng & Leal 1997). Other workers have also driven these shape modes directly by mechanically restraining bubbles in a wire loop and exciting an acoustic travelling wave in the kHz frequency range (Francescutto & Nabergoj 1978). Recent advances in the technique for ultrasonically trapping larger, millimetre-size bubbles have permitted the detailed analysis of certain aspects of the damping of their shape oscillatory dynamics (Asaki *et al.* 1993; Asaki, Thiessen & Marston

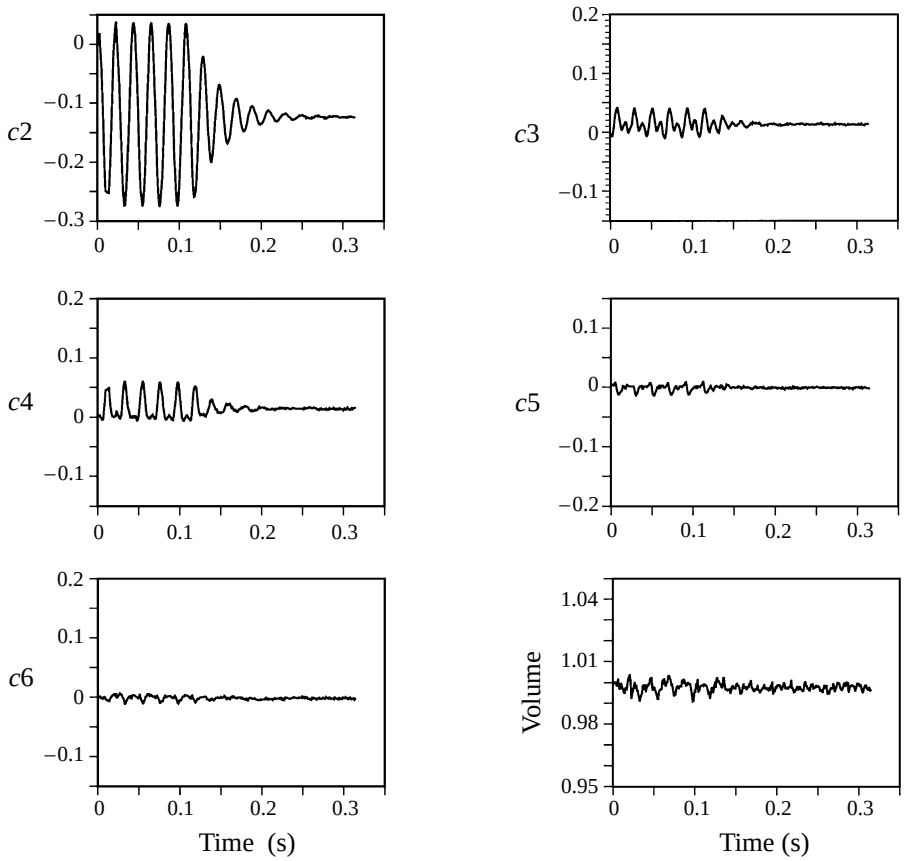

FIGURE 11. Time dependence of the Legendre coefficients for a 0.42 cm diameter air bubble trapped in water. The bubble is initially driven into the $l = 2$ mode and the oscillations are allowed to freely decay. Harmonics of the driving frequency can be detected, but an obvious characteristic is the presence of the driving frequency in the response of all the Legendre modes.

1995). In this paper, we report some quantitative measurements of the characteristics of large-amplitude shape oscillations of air bubbles several millimetres in diameter and trapped in distilled water.

3.2.1. *Shape oscillations of air bubbles acoustically trapped in water*

Air bubbles trapped by the 22.5 kHz standing wave were initially driven in one of the resonant shape modes and the subsequent freely decaying oscillations were analysed using modal decomposition in the same manner as described in previous sections for the case of drops. The initial oscillation amplitude was generally on the order of, or larger than, 10% of the equivalent equilibrium bubble radius. Our attention was mainly focused on the excitation of neighbouring resonant modes. The experimental time resolution for all the data sets presented below was 1 ms.

Figure 11 shows plots of the first five Legendre coefficients and of the volume as a function of time for a 0.42 cm diameter air bubble initially driven into the axisymmetric $l = 2$ resonant mode (49.5 Hz). The most notable higher-mode excitation at the appropriate characteristic resonance frequency is revealed by the response of the $l = 3$ mode. Dual frequency response is detected during both the driven and free-decay phases: both the driving frequency and roughly double that frequency are

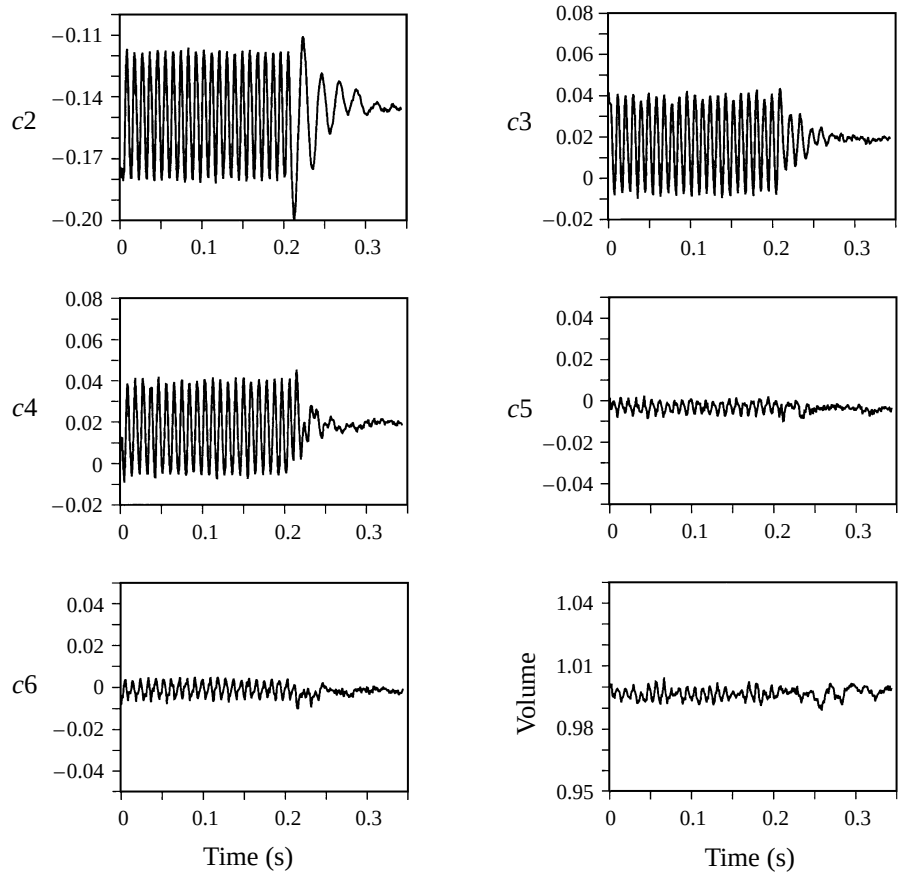

FIGURE 12. For caption see facing page.

clearly visible in the $c3$ time response curve. The evidence also shows that the $l = 4$, and to a much smaller extent the $l = 5$ and $l = 6$ shapes, were also excited at the same $l = 2$ frequency during the acoustically driven phase.

Figure 12 displays plots of the Legendre coefficients as a function of time for a 0.41 cm diameter air bubble initially driven into the axisymmetric $l = 3$ mode (83 Hz). As shown before, all the resonant shapes are excited at the single driving frequency in the steady-state regime. A characteristic nearly single frequency decay is measured for the $l = 2$ mode as soon as the acoustic drive is terminated, while both the $l = 3$ and $l = 4$ modes display a superposition of the $l = 2$ and of their characteristic normal mode free-decay frequencies. This is better shown in figure 13 where the Fourier transform of the time-series data in the free-decay region was performed. The lowest-order ($l = 2$) and the next higher ($l = 4$) modes frequencies are not harmonically related to the excitation frequency, the experimental results for the mode frequency ratios are $\omega 3/\omega 2 = 1.71$ and $\omega 4/\omega 2 = 2.43$. These values are lower than the linear theoretical predictions for ideal spherical bubbles of 1.82 and 2.74 respectively.

Figure 13 reports similar results except that the initial acoustic drive was for the $l = 4$ mode (136.5 Hz). Once again, the $l = 2$ natural free-decay frequency is present in all the Legendre coefficient time series, and each characteristic mode frequency

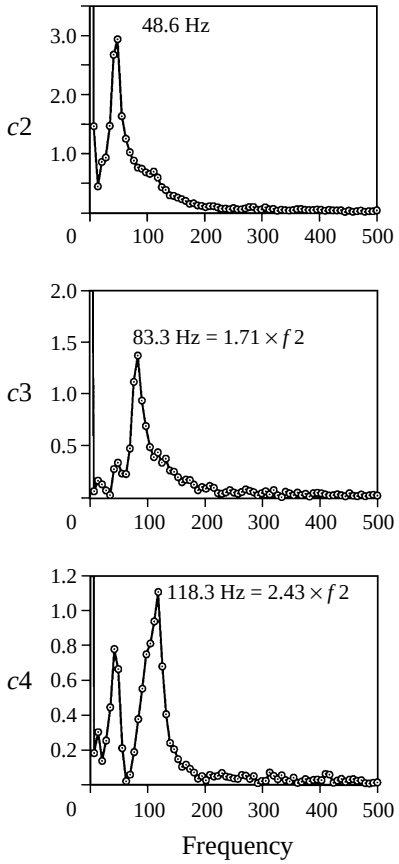

FIGURE 12. Time-dependence and FFT of the Legendre coefficients for a 0.41 cm diameter air bubble trapped in water and initially driven into its $l = 3$ resonant mode. All the modes respond at the forcing frequency during the driven phase, but the characteristic frequencies of the normal modes are recovered during the free-decay phase, although they are modulated by the least-damped $l = 2$ mode oscillations.

is generated in the free-decay phase. The freely decaying oscillations of the higher modes are thus modulated by the least-damped natural oscillations in the fundamental quadrupole mode.

4. Discussion and summary

Driven large-amplitude shape oscillations responses of drops and freely decaying oscillations of bubbles have been investigated in this work. Ample evidence for subharmonically and harmonically induced mode coupling has been documented for both drops and bubbles. This is at least in partial agreement with the theoretical predictions of Tsamopoulos & Brown (1984).

For drops, a significant result described here is the uncovering of an efficient subharmonic excitation of a resonant mode concurrent with the usual higher-harmonic excitation. The former is more efficient due to the increasingly greater viscous damping of shape oscillations with higher mode numbers. A certain degree of detuning has also been found to be acceptable for subharmonic excitation: exact matching of the natural resonance frequency of this secondary mode to half the drive frequency is not

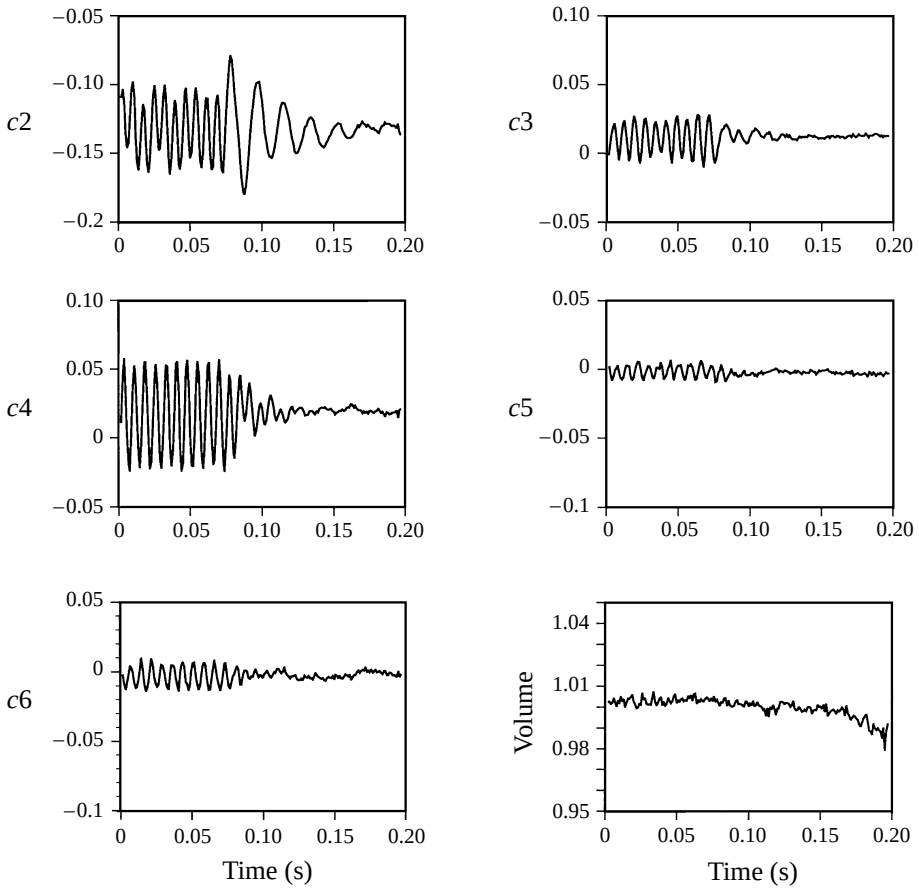

FIGURE 13. Time-dependence of the Legendre coefficients for an air bubble driven in its $l = 4$ resonant mode. All modal responses are at the driving frequency in the initial phase, but the characteristic modal frequencies are again recovered in the free-decay portion.

required. Also significant is the fact that a mode of different symmetry characteristics can be excited as long as its resonance frequency is close to half the drive frequency. Finally, all shape oscillation modes are driven at the excitation frequency, and it appears that even-numbered modes do not easily couple to odd-numbered ones, while odd-numbered modes can excite even modes. This is in agreement with previous theoretical work describing the dynamics of electrostatically levitated charged drops (Tsamopoulos & Brown 1984; Feng & Beard 1990, 1991).

In the case of bubbles, it is clear that the free-decay dynamics are dominated by the least-damped mode, regardless of the nature of the original driven mode. As is the case for drops, all the modes are driven at the excitation frequency, but the bubbles higher-order modes are found to freely decay at their characteristic resonant frequencies superposed on the fundamental mode frequency. The deformed, semi-oblate shape of these trapped bubbles is not symmetrical with respect to the equator. This non-spherical equilibrium shape could explain why the experimental ratios for the resonant mode frequencies are lower than the predictions from linear theory.

We have not been able to obtain direct mode-coupling data in the acoustically driven bubbles similar to those obtained for drops. This is perhaps due to our desire

to keep the acoustic field intensity low enough to avoid the excitation of high-frequency capillary waves on the bubble surface. The limitation of this particular experimental approach is thus more restricting in the case of bubbles. However, other evidence of mode coupling is clearer for the case of bubbles in the free-decay phase: all the appropriate resonant frequency components were detected regardless of which mode was initially excited. We believe that this set of data should be even more reliable since it is not influenced by the way the acoustic field modulates the drop shape.

Because of the need for levitation (or trapping) the fluid particles are not totally free. This is reflected in the oblate equilibrium shapes of the relatively large air bubbles studied here and in the outer-liquid streaming flows. The drops and bubbles are thus not completely free of external influence since they are constrained to remain at a fixed location by the sound field. It has been theorized that the equilibrium shape of the drop or bubble also plays a significant role in the mode coupling processes involved at large-amplitude oscillations. This may be intuitively understood once the shifting of the resonance frequencies by static shape deformation and removal of mode degeneracy is taken into account. The performance of the same experiments in low gravity where all positioning forces are turned off during the free-decay phase would provide results devoid of field interference, and it might provide a direct quantitative assessment of this bias.

Previous theoretical works dealing with weakly viscous drops have suggested a significant influence of viscosity on nonlinear mode coupling characteristics (Basaran 1992; Becker *et al.* 1993). The results reported here point to an obvious bias toward the secondary excitation of less-damped and harmonically related resonant modes during the active excitation of a primary mode at large amplitude. The apparent significant degree of detuning observed here also suggests the influence of viscous effects, although this may also emphasize the effect of the soft nonlinearity in the resonance frequencies.

This work was carried out at the Jet Propulsion Laboratory, California Institute of Technology under contract with the Microgravity Research Division of the National Aeronautics and Space Administration. We thank the referees for many helpful and insightful suggestions.

REFERENCES

Annamalai, P., Trinh, E. & Wang, T. G. 1985 Experimental study of the oscillations of a rotating drop. *J. Fluid Mech.* **158**, 317–327.

Apfel, R. E. 1976 Technique for measuring the adiabatic compressibility, density, sound speed of sub-microliter liquid samples. *J. Acoust. Soc. Am.* **59**, 339–344.

Asaki, T. J., Marston, P. L. & Trinh, E. H. 1993 Shape oscillations of bubbles in water driven by modulated ultrasonic radiation pressure: observations and detection with scattered laser light. *J. Acoust. Soc. Am.* **93**, 706–713.

Asaki, T. J., Thiessen, D. B. & Marston, P. L. 1995 Effects of an insoluble surfactant on capillary oscillations of bubbles in water: observation of a maximum in damping. *Phys. Rev. Lett.* **75**, 2686–2689.

Azuma, H., Yoshihara, S. & Ohnishi, M. 1989 An experimental study of electrically excited liquid-drop oscillations. *40th Congr. Intl Astronautical Federation* 89-448.

Basaran, A. O. 1992 Nonlinear oscillations of viscous liquid drops. *J. Fluid Mech.* **241**, 169–198.

Becker, E., Hiller, W. J. & Kowalewski, T. A. 1994 Nonlinear dynamics of viscous droplets. *J. Fluid Mech.* **258**, 191–216.

Benjamin, T. B. & Ellis, A. T. 1990 Self-propulsion of asymmetric vibrating bubbles. *J. Fluid Mech.* **212**, 65–80.

Blass, E. 1990 Formation and coalescence of bubbles and droplets. *Intl Chem. Engng* **30**, 206–221.

Eller, A. I. 1968 Force on a bubble in a standing acoustic wave. *J. Acoust. Soc. Am. Lett.* **43**, 170–171.

Eller, A. I. & Crum, L. A. 1970 Instability in the motion of a pulsating bubble in a sound field. *J. Acoust. Soc. Am.* **47**, 762–770.

Feng, J. Q. & Beard, K. V. 1990 Small-amplitude oscillations of electrostatically levitated drops. *Proc. R. Soc. Lond.* A **430**, 133–150.

Feng, J. Q. & Beard, K. V. 1990 Three-dimensional oscillations of electrostatically deformed drops. *J. Fluid Mech.* **227**, 429–445.

Feng, Z. C. & Leal, L. G. 1997 Nonlinear bubble dynamics. *Ann. Rev. Fluid Mech.* **29**, 201–243.

Francescutto, A. & Nabergoj, R. 1978 Pulsation amplitude threshold for surface waves on oscillating bubbles. *Acustica* **41**, 215–220.

Holt, R. G. & Gaitan, D. F. 1996 Observation of the stability boundaries in the parameter space of single-bubble sonoluminescence. *Phys. Rev. Lett.* **77**, 3791–3797.

Holt, R. G. & Trinh, E. H. 1994 Radiation pressure-induced capillary waves. *J. Acoust. Soc. Am.* **95**, 2988.

Kaji, N., Mori, Y. H., Tochitani, Y. & Komotori, K. 1985 Heat transfer enhancement due to electrically-induced resonant oscillations of drops. *J. Heat Transfer* **107**, 788–792.

Kawalski, W. & Ziolkowski, Z. 1981 Increase in rate of mass transfer in extraction columns by means of an electric field. *Intl Chem. Engng* **21**, 323–335.

Lamb, H. 1881 On the oscillations of a viscous spheroid. *Proc. Lond. Math. Soc.* **13**, 51–56.

Marston, P. L. 1980 Shape oscillations and static deformation of drops and bubbles driven by modulated radiation-pressure-Theory. *J. Acoust. Soc. Am.* **67**, 15–26.

Marston, P. L. & Apfel, R. E. 1979 Acoustically-forced shape oscillations of hydrocarbon drops levitated in water. *J. Colloid Interface Sci.* **68**, 280–286.

Miller, C. A. & Scriven, L. E. 1968 The oscillations of a fluid droplet immersed in another fluid. *J. Fluid Mech.* **32**, 417–435.

Natarajan, R. & Brown R. A. 1986 Quadratic resonance in the three-dimensional oscillations of inviscid drops with surface tension. *Phys. Fluids* **29**, 2788–2797.

Prosperetti, A. 1980 Normal mode analysis for the oscillations of a viscous liquid drop immersed in another liquid. *J. Méc.* **19**, 149–182.

Rayleigh, Lord 1879 On the capillary phenomena of jets. *Proc. R. Soc. Lond.* **29**, 71–97.

Rhim, W. K., Elleman, D. D. & Saffren, M. 1982 Normal modes of a compound drop. In *Proc. Second Intl Conf. on Drops and Bubbles, Monterey, CA* (ed. D. LeCroissette). NASA-JPL publication 82-7, pp. 7–14.

Scott, T. C., Basaran, A. O. & Byers, C. H. 1990 Characteristics of electric field-induced oscillations of translating liquid droplets. *Ind. Engng Chem. Res.* **29**, 901–909.

Shi, T. & Apfel, R. E. 1995 Oscillations of a deformed liquid drop in an acoustic field. *Phys. Fluids* **7**, 1545–1552.

Strasberg, M. & Benjamin, T. B. 1958 Excitation of the oscillations in the shape of pulsating gas bubbles. *J. Acoust. Soc. Am.* **30**, 697.

Suryanarayana, P. V. R. & Bayazitoglu, Y. 1991 Surface tension and viscosity from damped free oscillations of viscous droplets. *Intl J. Thermophys.* **12**, 137–151.

Trinh, E. H., Holt, R. G. & Thiessen, D. B. 1996 The dynamics of ultrasonically levitated drops in an electric field. *Phys. Fluids* **6**, 3567–3579.

Trinh, E. & Wang, T. G. 1982 Large-amplitude free and driven drop-shape oscillations: experimental results. *J. Fluid Mech.* **122**, 315–338.

Trinh, E., Zwern, A. & Wang, T. G. 1982 An experimental study of small-amplitude drop oscillations in immiscible liquid systems. *J. Fluid Mech.* **115**, 453–474.

Tsamopoulos, J. A. & Brown, R. A. 1983 Nonlinear oscillations of inviscid drops and bubbles. *J. Fluid Mech.* **127**, 519–537.

Tsamopoulos, J. A. & Brown, R. A. 1984 Resonant oscillations of inviscid charged drops. *J. Fluid Mech.* **147**, 373–395.

Wright, H. & Ramkrishna, D. 1994 Factors affecting coalescence frequency of droplets in a stirred liquid-liquid dispersion. *AIChE J.* **40**, 767–776.